Effects of atmospheric gases on Li metal cyclability and solid-electrolyte interphase formation

Experimental methods and supplemental information

*Evelyna Wang[a], Sunita Dey[a], Tao Liu[a], Svetlana Menkin[a], Clare P. Grey[a]**

AUTHOR ADDRESS

[a]Department of Chemistry, University of Cambridge, Lensfield Road, Cambridge CB2 1EW, UK

AUTHOR INFORMATION

Corresponding Author

**cpg27@cam.ac.uk*

Fax: (+44)1223336362; Tel: (+44)1223336509

Experimental Methods. Li|Cu Swagelok cells were assembled in an Ar-filled glovebox (fig S1). Copper mesh was used to enable gas diffusion into the electrolyte and therefore participate in SEI forming reactions. Current densities of 0.25 mA/cm^2 (real surface area) were used: Cu mesh electrodes with diameter of 10 mm were used (geometric area = 0.78 cm^2). The real surface area, subtracting out void space, was calculated using image processing software (real area = 0.45 cm^2). Current used was 0.11 mA. Gas pressures were static at 1.5-2 bar. Electrochemical tests were performed using a Biologic Potentiostat.

In order to avoid H_2O contamination, all cell components were sonicated in ethanol and then dried in a 60ºC oven. Cell components were left under vacuo for 1 hr prior to cell assembly in the glovebox. N6.0 gas purities were used for electrochemical mass spectrometry and N3.0 gas purities were used for all other tests. Gas lines were kept under vacuum for 30 min prior to filling cells.

Cells were disassembled in an Ar-filled glovebox. Copper electrodes were rinsed with dimethyl ether and dried under vacuo prior to characterization. Scanning Electron Microscopy (SEM) was performed on a Tescan MIRA3 at 5 keV accelerating voltage. Samples were transferred from the glovebox using a Kammarth and Weiss transfer module. Electron dispersive X-ray Spectroscopy (EDX) was performed using an Oxford Instruments probe with AZtec software. X-ray diffraction (XRD) was performed using a PANalytical Empyrean diffractometer in reflection mode (Cu K α1 radiation) with Bragg-Brentano geometry. Samples were sealed between Kapton sheets. Fourier Transform Infrared (FTIR) was performed in the Ar glovebox using an Agilent Cary 630 spectrometer. X-ray Photoelectron Spectrometry (XPS) was performed using a Thermo Fischer Scientific instrument with monochromated Al-K alpha X-ray source using an air-sensitive transfer module. The XPS data was calibrated by setting the adventitious carbon C-C peak to 284.8 eV.

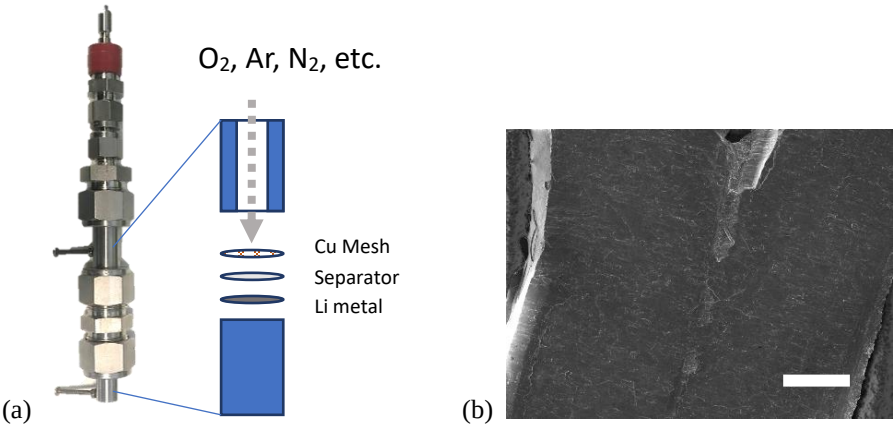

Supplemental figure 1: (a) Schematic of cell assembly with Swagelok design, ½" diameter. (b) SEM image of the Cu mesh. Scale bar = 50 μm.

A Li metal foil was used as the counter and reference electrode. Celgard 2400 swollen with 1M LiTFSI in tetraglyme was used as the separator and electrolyte. Copper mesh used as the substrate and working electrode for Li plating/stripping tests. A flat mesh was used, and current densities were calculated for the projected top-view area. A mesh was used to allow gas dissolution into the electrolyte.

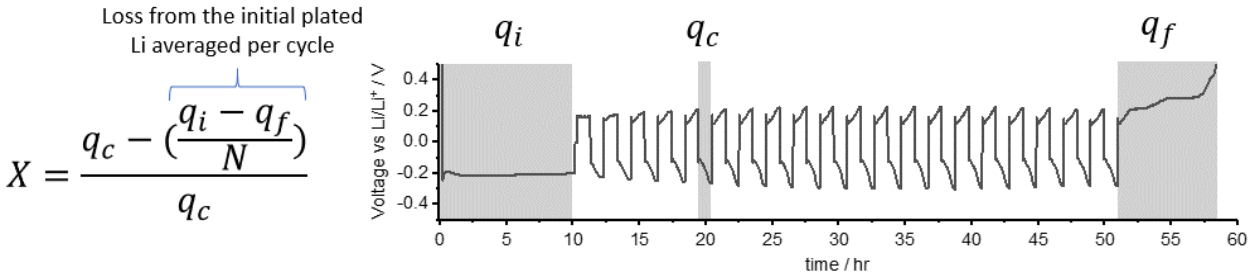

Supplemental figure 2: Method for calculating coulombic efficiencies

Coulombic efficiency was calculated using the Aurbach method.[1] This method considers an average coulombic efficiency over the whole experiment. First an initial quantity of lithium is plated onto the Cu (q_i). A fraction of this reservoir (q_c) is subjected to N cycles of symmetric plating and stripping. Finally, all available Lithium is stripped from the Cu (q_f). The coulombic efficiency, X, can then be calculated using the expression shown on the top left-hand side.

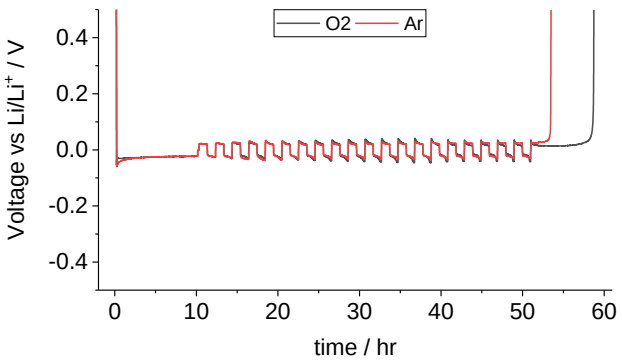

Supplemental figure 3: Voltage vs time plot for Li metal deposition using commercial battery grade (carbonate) LP30 electrolyte (1M $LiPF_6$ in 1:1 EC/DEC). An improvement in coulombic efficiency is observed in the presence of O_2. Plating overpotentials were similar to that in an Ar environment. This is consistent with our hypothesis that O_2 reduction occurs on the Cu electrode prior to Li plating, thus promoting uniform initial Li nucleation and growth.

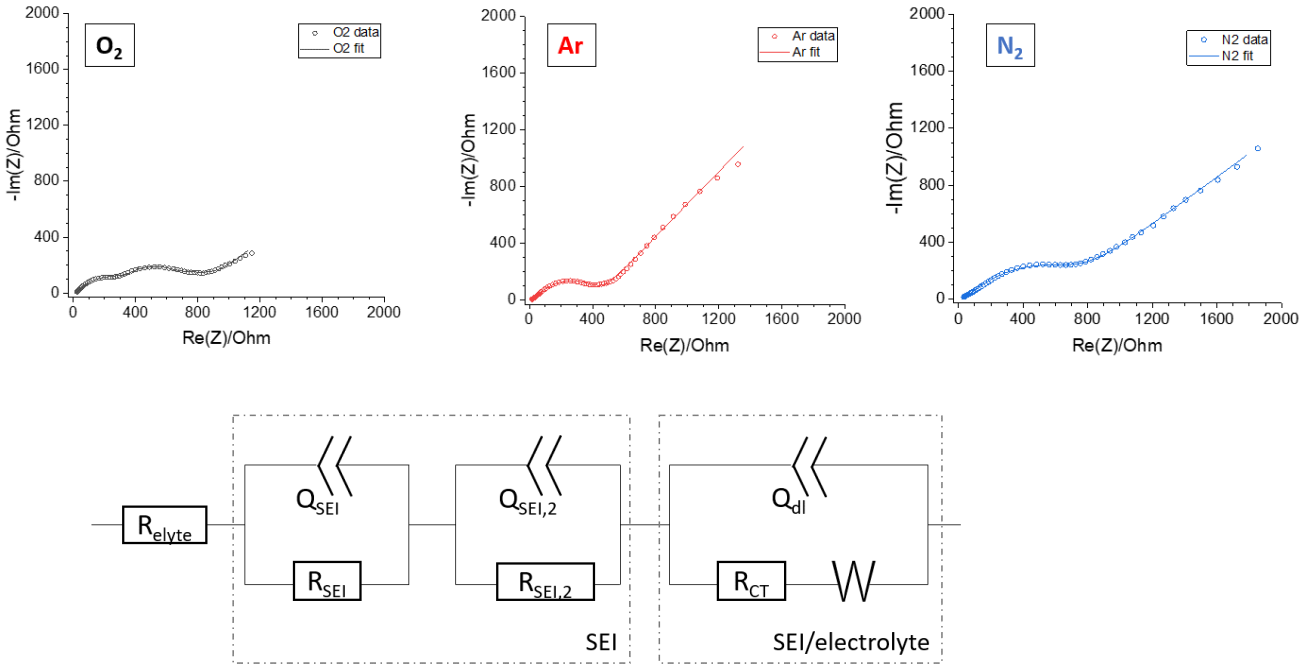

Supplemental figure 4: Electrochemical Impedance spectroscopy measured after 20 plating/stripping cycles in O_2, Ar, and N_2 environments (top) and equivalent circuit model used to fit the data (bottom).

A symmetric cell was made using the Cu working electrodes from two cycled cells. Potentiostatic EIS was performed from 1MHz to 1Hz using 10 mV amplitude. The poly-hetero microphase equivalent circuit from Peled et al. was adapted to model the EIS data.[2] Two capacitor/resistor elements were used to model the SEI, one for the interphase resistance and

capacitance, the other may refer to SEI grain boundary (SEI-2) resistance and capacitance. This second resistor/capacitor (RC) unit, connected in series, was necessary to fit the data, suggesting an additional component to the SEI layer with uniquely large resistance values in the O_2 sample (table S1 below). This RC unit has significantly higher capacitance (~10^{-5} F) than a typical grain boundaries capacitance (~10^{-8} -10^{-8} F),[3] however since the high-frequency semi-circle is usually assigned to the contribution of grain boundaries, this component likely corresponds to the LiOH layer with large grain sizes (as seen in the SEM, fig S12). The high capacitance could be the result of higher porosity compared to the typical porosity of ceramic electrolytes.[4]

A third capacitor/resistor element was used to model the charge transfer resistance (CT) and double layer capacitance (dl) at the SEI/electrolyte interface. A Warburg diffusion element was used to model Li ion diffusion.
Constant phase elements were used instead of capacitors in order to capture the distribution of relaxation times caused by the complexity of the SEI layer.[5] These elements give a pseudocapacitance (Q) and the dispersion coefficient (a) refers to the phase deviation from 90 (an ideal capacitor).

Supplemental table 1: Summary of resistance and capacitance values from the EIS equivalent circuit model. The SEI-GB component showed differences in resistance for the O_2 sample, likely caused by the insulating LiOH layer. The dramatic increase in the Warburg diffusion for the N_2 sample may be an artifact of cell assembly.

			O_2	Ar	N_2
$R_{electrolyte}$	Ω	Resistance of bulk electrolyte	20.31	11.99	17.71
R_{SEI}	Ω	Resistance of bulk SEI layer	354	389.8	402.4
Q_{SEI}	$F*s^{(a-1)}$	Pseudocapacitance of SEI layer	9.87 e-06	1.32 e-05	1.24 e-05
a_{SEI}		Dispersion coefficient for SEI capacitance	0.6402	0.7089	0.6517
R_{SEI-2}	Ω	Resistance of grain boundaries in the SEI or secondary layer	192.9	38.7	127.2
Q_{SEI-2}	$F*s^{(a-1)}$	Pseudocapacitance of grain boundaries in the SEI or secondary layer	1.89 e-05	8.11 e-05	3.39 e-05
a_{SEI-2}		Dispersion coefficient for grain boundaries in the SEI or secondary layer	1	0.4884	0.8721
$R_{CT-SEI/electrolyte}$	Ω	Resistance of charge-transfer at the SEI/electrolyte interface	333.8	94.91	238
$Q_{dl-SEI/electrolyte}$	$F*s^{(a-1)}$	Pseudocapacitance for the electric double layer formed at the SEI/electrolyte interface	2.22 e-04	2.74 e-04	2.19 e-04
a_{dl}		Dispersion coefficient for the electric double layer formed at the SEI/electrolyte interface	0.785	0.7634	0.7818
W	$\Omega *s^{-1/2}$	Warburg diffusion element	231.3	1024	4837
Fit			0.019	0.022	0.057

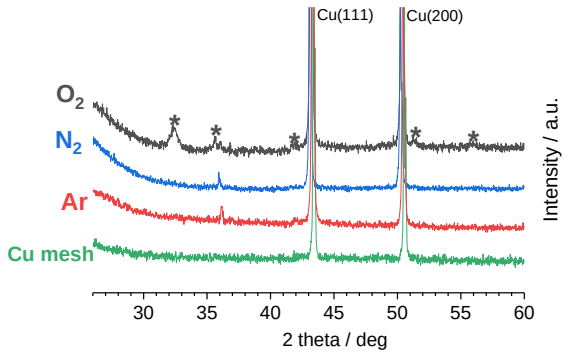

Supplemental figure 5: XRD characterization of the Cu electrode after cycling and stripping all available lithium. Li metal peaks at ~ 36.5º were observed in Ar and N_2 samples, indicating dead Li trapped in the remaining SEI. LiOH peaks marked by "*" were seen only of the O_2 samples.

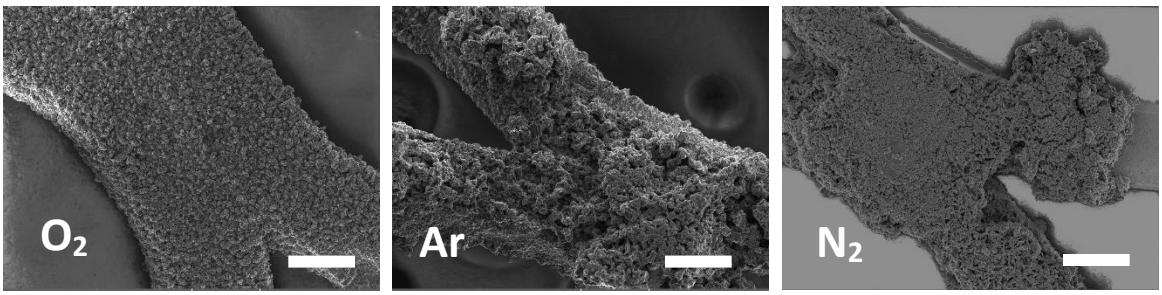

Supplemental figure 6: SEM images of the cycled Li metal at a lower magnification than fig 2 in the main text. Scale bar = 100 um.
Samples cycled in an O_2 environment (left) displayed more homogeneous morphologies on the Cu mesh, while Ar (middle) and N_2 (right) showed porous morphologies as well as localized deposition where regions of bare Cu can still be visible.

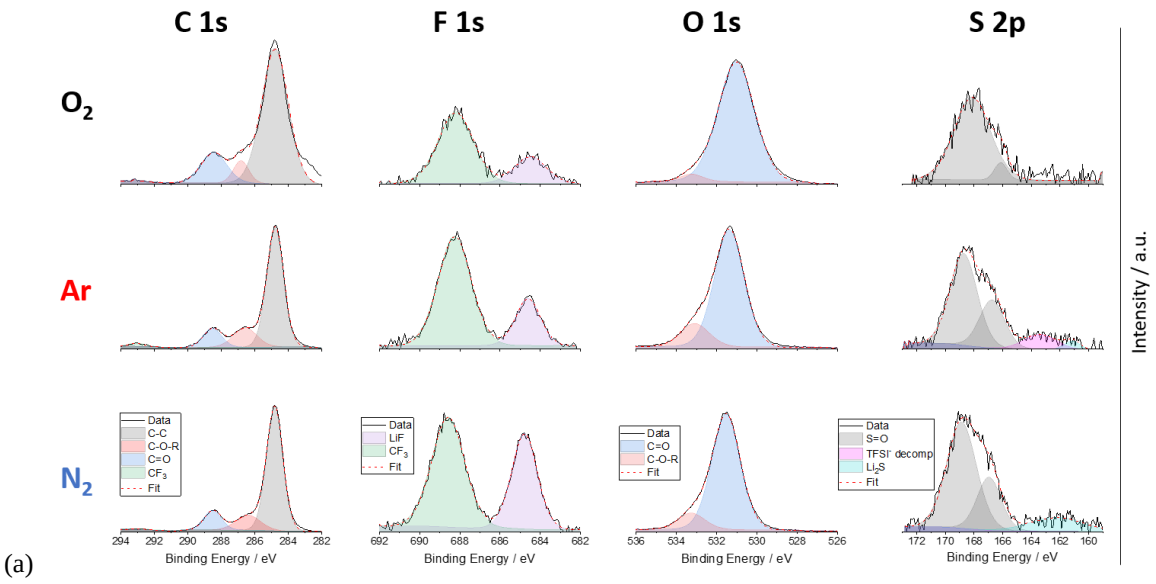

(a)

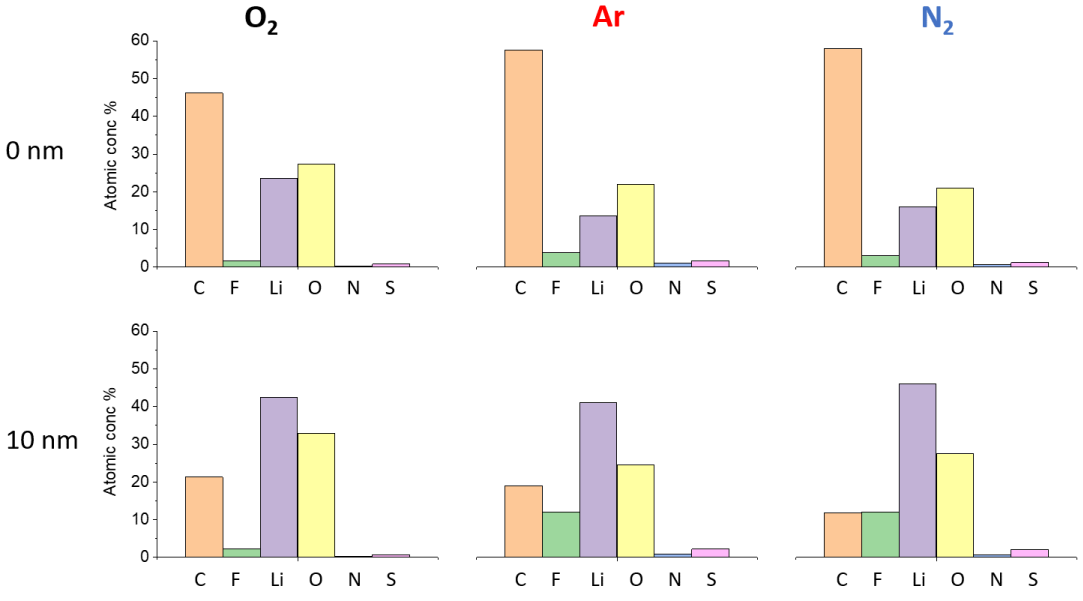

(b)

Supplemental figure 7: (a) The C 1s, F 1s, O 1s, and S 2p XPS spectra for the SEI formed in various gas environments taken at the surface with no sputtering. (b) Histograms showing the relative atomic % from XPS measurements for the SEI formed in O_2, Ar, and N_2 at 0 nm and 10 nm sputtering depth. A large C-C peak is visible for all samples, indicative of adventitious carbon as well as the organic SEI layer. Small amounts of salt decomposition products such as LiF (purple) and Li_2S (cyan) and higher concentrations of F, N, and S were already visible, for Ar and N_2 samples.

Supplemental Table 2: Total atomic % for the SEI formed in O_2, Ar, and N_2 at various sputter depths.

		C	F	Li	O	N	S
Ar	0 nm	57.61	3.81	13.63	22.06	1.17	1.72
	10 nm	18.98	12.1	41.15	24.57	0.96	2.23
	20 nm	12.95	10.41	48.35	25.43	0.88	1.98
O_2	0 nm	46.19	1.68	23.66	27.34	0.32	0.8
	10 nm	21.34	2.26	42.49	32.88	0.3	0.73
	20 nm	17.26	2.43	45.94	33.38	0.27	0.71
N_2	0 nm	58.01	2.99	15.99	21.05	0.74	1.23
	10 nm	11.77	12.06	45.98	27.48	0.6	2.09
	20 nm	8.09	9.16	51.83	28.82	0.6	1.51
O_2/N_2 25:75	0 nm	50.46	3.02	19.49	23.04	2.28	1.82
	10 nm	10.98	11.35	46.13	28.38	1.1	2.06
	20 nm	9.59	10.67	48.29	28.61	0.96	1.88

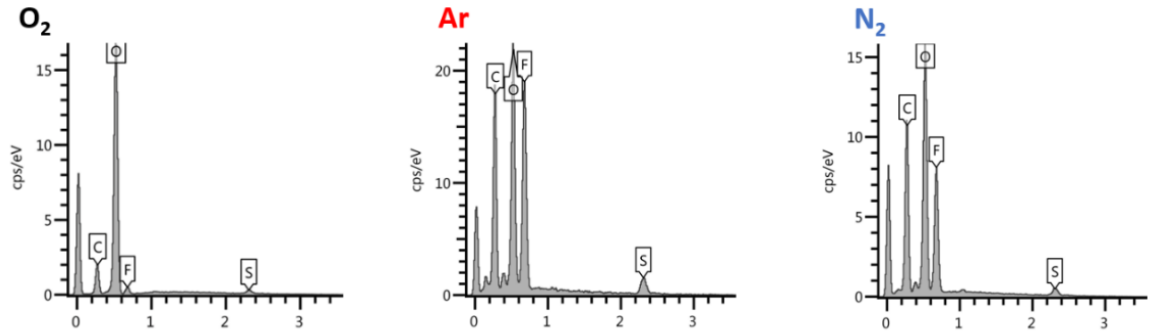

Supplemental figure 8: EDX spectra for SEI formed in O_2, Ar, and N_2. Significantly higher F and S content were observed for Ar samples.

Supplemental table 3: Relative atomic weight % from EDX point measurements of the SEI formed in various gas conditions. EDX spectra for Li metal exposed to O_2 and Ar at OCV with electrolyte were also measured.

For the electrochemically formed SEI in O_2, the O content was dramatically increased, while the chemically formed surface showed much less oxidation. The relatively high F content for Li metal exposed to O_2 and Ar at OCV is likely due to residual electrolyte.

	C	**F**	**O**	**S**	**N**
O_2	16.4	14.1	63.8	5.7	--
Ar	29.3	32.0	28.8	9.9	--
N_2	29.3	27.1	37.8	5.8	--
O2/N2 (25:75)	30.4	26.4	34.9	8.3	--
O2/N2 (75:25)	7.1	11.8	75.7	5.4	--
O_2 at OCV	31.4	31.7	33.9	--	3
Ar at OCV	37	33.2	27.2	--	2.5

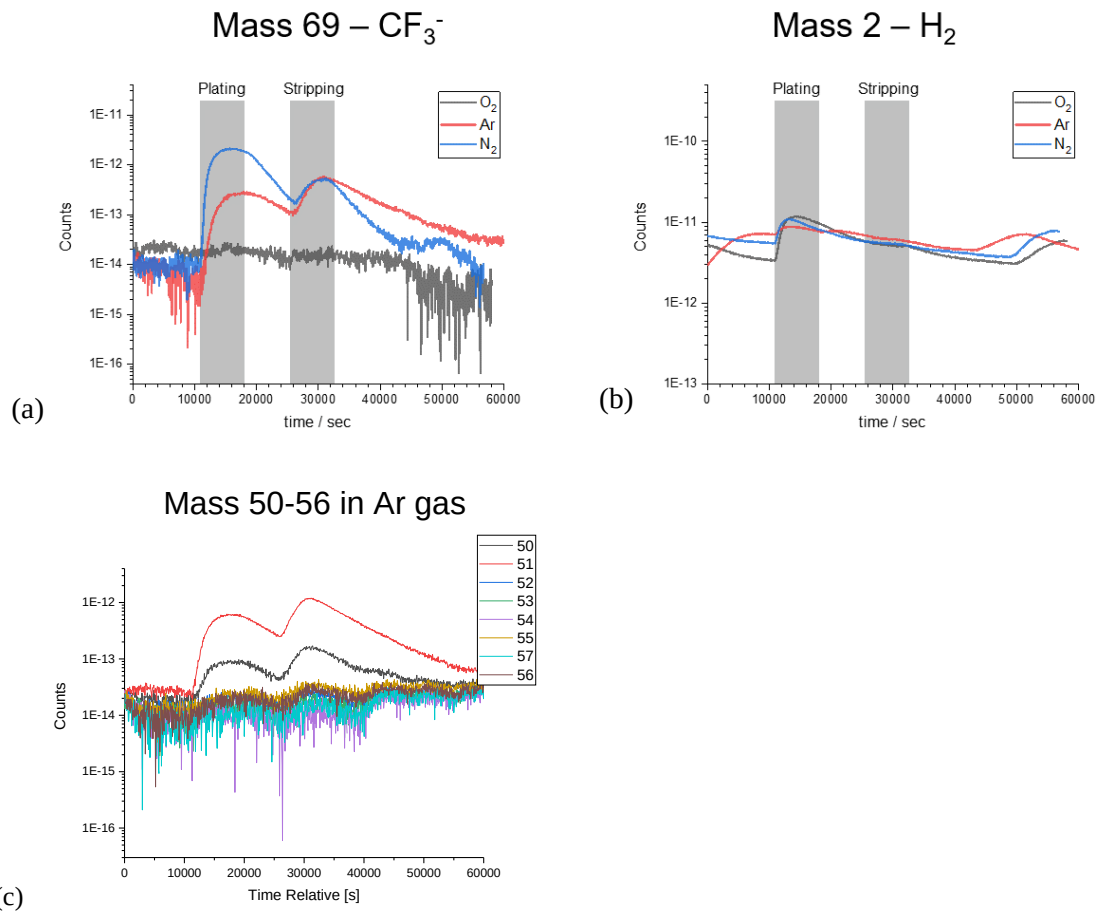

Supplemental figure 9: Online mass spectrometry data for SEI formed in O_2, Ar, and N_2: lithium was plated/stripped onto Cu mesh while atmospheric gas was flowed through the cell to the mass detector. (a) Comparison of mass 69 -CF_3 and (b) mass 2 -H_2 evolution in different gas environments. (c) Evolution of mass 50-56 in an Ar environment.

A dramatic increase in counts for mass 69 were detected at the onset of plating in Ar and N_2 environments, corresponding to CF_3^- species, which result from $TFSI^-$ anion decomposition. During the rest period between plating and stripping, the signal decreased.

Comparable amounts of H_2 gas were evolved from all samples, which may be formed from H_2O reaction with Li metal, indicating similar quantities of H_2O contamination for all samples. The mass spectroscopy data focusing on 50 & 51 amu for an Ar environment highlights the increased amounts of -CF_2 and -HCF_2 type species.

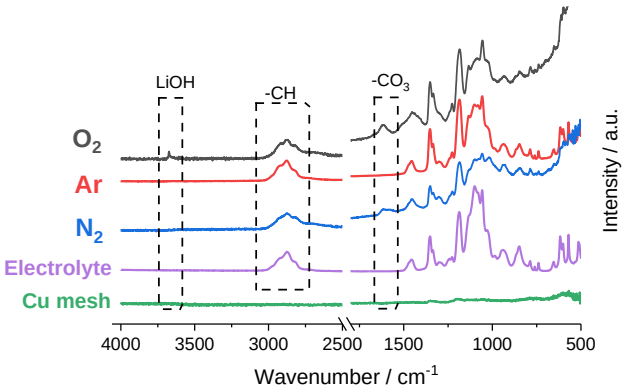

Supplemental figure 10: FTIR of lithium metal cycled in O_2, Ar, and N_2 gas environments. Bare Cu mesh and pristine electrolyte were measured as control samples. From the FTIR, a clear -OH peak corresponding to LiOH was only observed in O_2 samples.

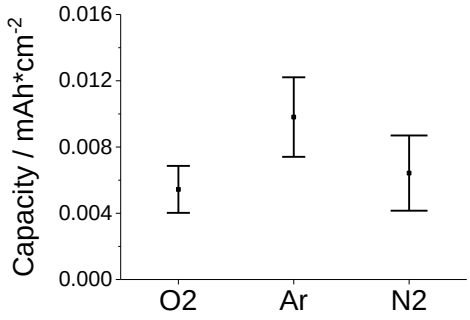

Supplemental figure 11: Extracted capacities for initial SEI formation prior to Li deposition. Error bars show standard deviations for 4 repeated cells in each gas environment.

As current is applied, various electrolyte species are reduced on the copper electrode until the potential drops to below 0 when Li^+ reduction begins. In the presence of O_2, less charge is needed to form a stable and electrically insulating initial layer.

(a) 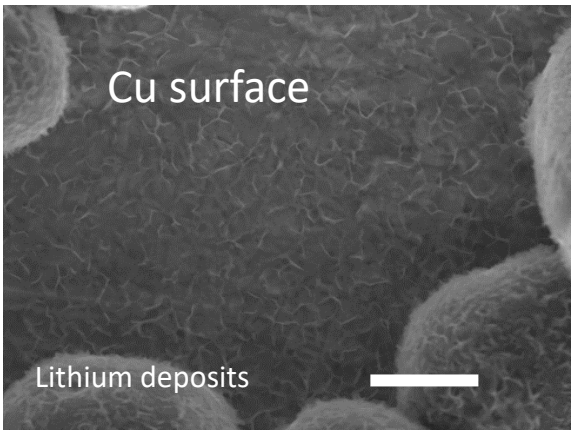

(b) 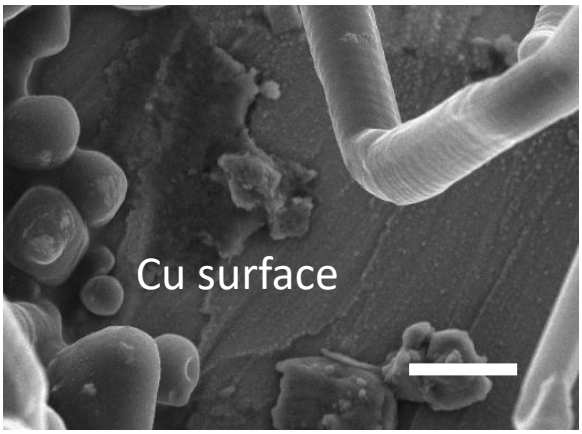

Supplemental figure 12: (a) SEM image of the Cu surface after plating Li (2.5mAh/cm^2) in an O_2 environment and (b) in an Ar environment. Scale bar = 2 um.

Flake like LiOH morphologies visibly cover the entire Cu surface when plating in an O_2 environment. LiOH flake-structures were visible on the surface of lithium nuclei as well. These are not observed when plating lithium in an Ar environment and the natural surface features of the Cu are still visible.

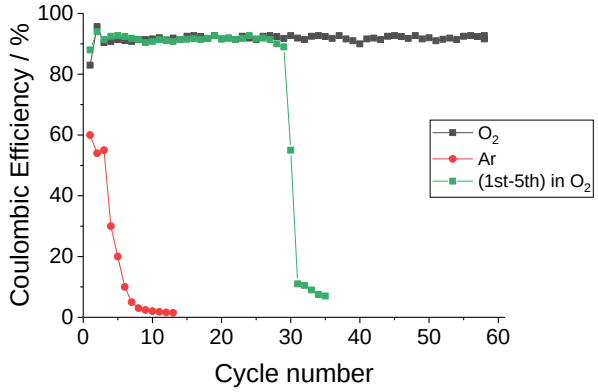

Supplemental figure 13: (a) Coulombic efficiency as a function of cycle number for symmetric plating/stripping in Li|Cu cells for different gas environments.

The cell in an O_2 environment shows consistent coulombic efficiencies for many cycles (black). In an Ar environment, coulombic efficiency drops rapidly after the first 3 cycles due to dead Li (red). Cycle life could be greatly improved when 5 plating/stripping cycles were first performed under an O_2 environment before purging the cell with Ar gas and continuing to cycle in an Ar environment (green). However, even with the pre-treatment, the coulombic efficiency drops after 30 cycles.

(a)

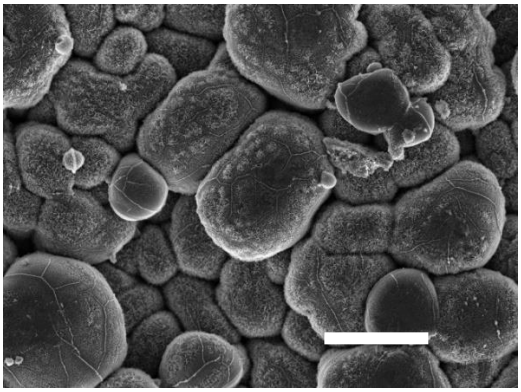

(b)

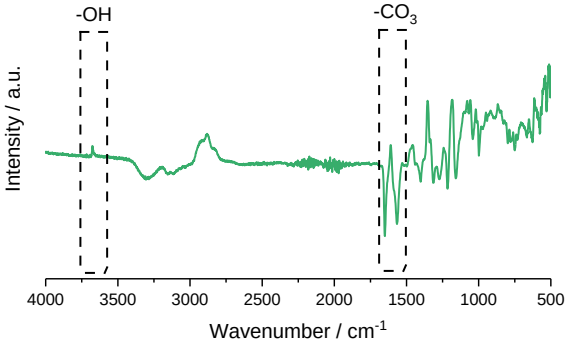

Supplemental figure 14: (a) SEM image of Li plating after 2.5mAh/cm^2 in O_2/N_2 50:50 environment. Scale bar = 10 um. (b) FTIR spectra for SEI formed in O_2/N_2 (25:75) environment.

LiOH is visible on the surface of the Li nuclei and the FTIR show peaks for both -OH (~3650 cm^{-1}) and -CO_3 (~1620 cm^{-1}) in mixed O_2/N_2 environments.

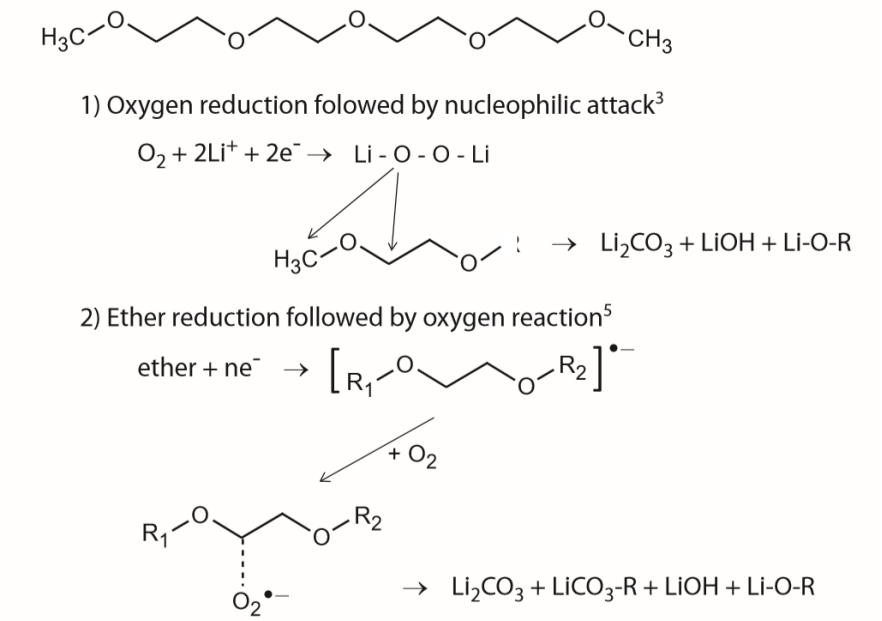

Supplemental figure 15: Schematic of possible glyme decomposition methods.

(1) Oxygen is reduced into Li-oxide species which can nucleophilically attack ethers and form Li-carbonates, Li-alkoxys, and LiOH.[6]
(2) Ether reduction to form a radical which is readily stabilized by O_2 forming a peroxy- radical. DFT calculations performed by Assary et al. indicate that the O_2 reaction with ether radical is favorable.[7] The radical then decomposes into Li-carbonates, Li-alkoxys, and LiOH.

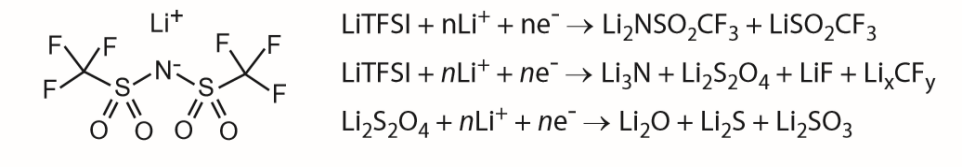

Supplemental figure 16: Possible LiTFSI reduction mechanisms.[8] The N-S and S-F bond cleavages are highly possible under the reductive conditions of Li plating.[9]

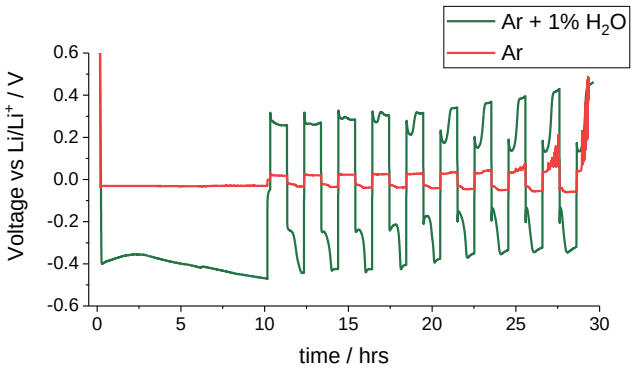

(a)

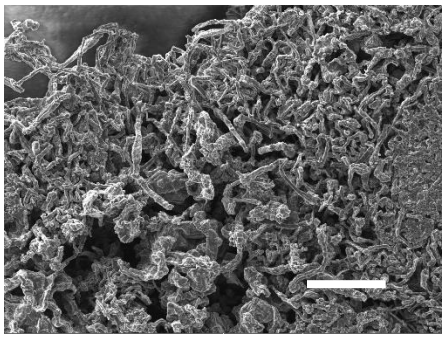

(b)

Supplemental figure 17: (a) Potential vs time plot for Li|Cu cells cycled in an Ar environment with 1% H_2O added into the electrolyte. (b) SEM image of cycled morphology after stripping all available lithium with H_2O added. Scale bar = 50 um.

Additional experiments adding 1% H_2O into the electrolyte and then plating/stripping lithium in an Ar environment were performed. Cells were only able to complete 9 symmetric plating/stripping cycles before a final stripping step to remove all available lithium: coulombic efficiencies calculated using the Aurbach method were 40% and 42% for the Li cycled in Ar and Ar with H_2O additive, respectively. This suggests that although H_2O contamination may form LiOH in the SEI, it does not appear to affect Li plating/stripping efficiencies in the same manner as O_2 crossover species. Future experiments using deuterated glymes may be explored to confirm the proton source in the LiOH found in the SEI. Dendrites are still visible in the SEM image even with the addition of water, explaining the low coulombic efficiencies even with water additive.

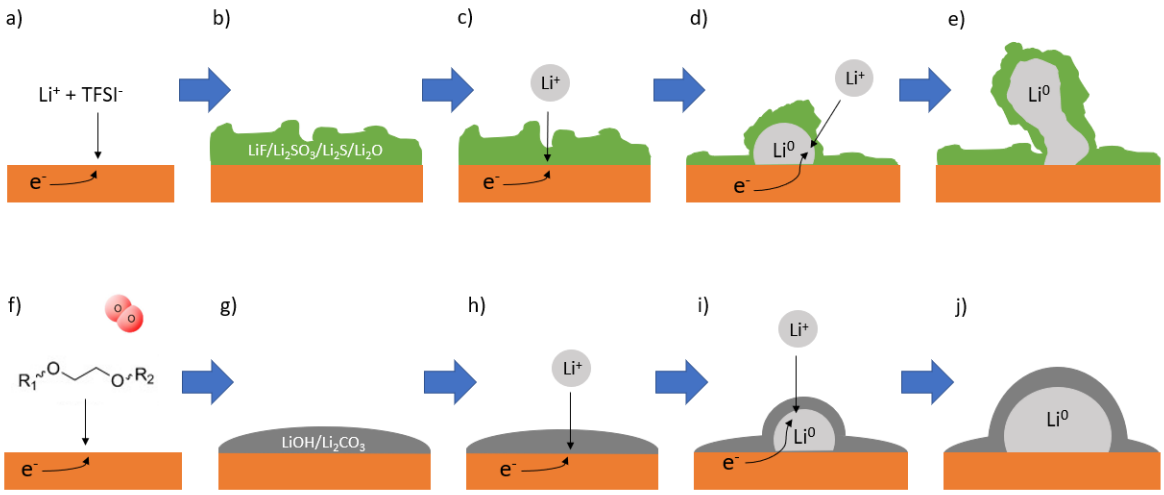

Supplemental figure 18: Schematic of SEI formation and initial Li nucleation in an Ar environment (a-e) compared to an O_2 environment (f-j).

Electrolyte is first reduced until the Cu electrode is uniformly covered by an electrically insulating layer that prevents further electrolyte reduction (a, f). The O_2 crossover species may help form a uniform coating of LiOH and Li carbonates (g) compared to an SEI composed of heterogeneous salt decomposition products (b). Lithium ions then migrate through the SEI in order to be reduced to Li metal (c-d, h-i). The SEI formed with O_2 is more robust and uniform, therefore promotes spherical growths (e, j).

Supplemental Table 4: Peaks in the C 1s spectra for SEI formed in O_2, Ar, and N_2 at various sputter depths. Li_2CO_3 is seen as an SEI component ~290 eV and is in larger relative concentrations for samples in O_2. The CF_3 peaks seen at the surface is due to residual $TFSI^-$ salt anion or decomp products.

Environment	Depth	Assignment	Position (eV)	%At Conc	
Ar	0 nm	C-C	284.77	40.2	
		C-O	286.55	8.95	
		C=O	288.52	7.2	
		CF_3	293.02	1.02	57.61
	10 nm	C-C	284.71	14.01	
		C-O	286.78	2.06	
		C=O	288.49	2.53	
		Li_2CO_3	290.03	0.38	18.98
	20 nm	C-C	284.73	9.11	
		C-O	286.75	1.57	
		C=O	288.49	1.65	
		Li_2CO_3	289.93	0.62	12.95
O_2	0 nm	C-C	284.78	35.01	
		C-O	286.8	3.39	
		C=O	288.43	7.79	46.19
	10 nm	C-C	284.75	10.83	
		Li-C	283.03	2.97	
		C=O	287.67	4.97	
		Li_2CO_3	290.24	2.57	21.34
	20 nm	C-C	284.7	10.9	
		Li-C	283	1.1	
		C=O	288.43	2.76	
		Li_2CO_3	290.44	2.5	17.26
N_2	0 nm	C-C	284.8	42.45	
		C-O	286.38	7.83	
		C=O	288.5	7.38	
		CF_3	292.77	0.35	58.01
	10 nm	C-C	284.8	7.43	
		C-O	287.1	1.1	
		C=O/(C=O)OR	288.92	2.06	
		Li_2CO_3	290.13	1.18	11.77
	20 nm	C-C	284.77	4.94	
		C-O	286.89	0.46	
		C=O	288.28	1.2	
		Li_2CO_3	290	1.49	8.09
O_2/N_2 (25:75)	0 nm	C-C	284.8	33.63	
		C-O	286.58	8.84	
		C=O	288.6	6.25	
		CF_3	292.58	1.74	50.46
	10 nm	C-C	284.86	6.25	
		C-O	287.03	2.52	
		C=O	288.54	0.8	
		Li_2CO_3	289.94	1.41	10.98
	20 nm	C-C	284.8	4.87	
		C-O	286.92	1.65	
		C=O	288.68	1.85	
		Li_2CO_3	289.98	1.22	9.59

Li pristine	C-C	284.81	51.7	
	C-O	286.91	2.37	
	C=O	288.49	4.57	58.63
Li + electrolyte + O_2	C-C	284.8	16.63	
	C-O	286.58	8.13	
	C=O	288.78	4.12	
	CF_3	293.01	2.23	31.11

Supplemental Table 5: Peaks in the F 1s spectra for SEI formed in O_2, Ar, and N_2 at various sputter depths. LiF can be clearly seen at all depths ~685eV.

Environment	Depth	Assignment	Position (eV)	%At Conc	
Ar	0 nm	LiF	684.6	0.93	
		CF_3	688.26	2.88	3.81
	10 nm	LiF	685.67	11.26	
		CF_3	688.76	0.84	12.1
	20 nm	LiF	684.97	9.36	
		CF_3	686.5	1.05	10.41
O_2	0 nm	LiF	684.48	0.43	
		CF_3	688.20	1.25	1.68
	10 nm	LiF	685.63	2.08	
			688.87	0.18	2.26
	20 nm	LiF	685.66	2.43	2.43
N_2	0 nm	LiF	684.78	1.2	
		CF_3	688.58	1.79	2.99
	10 nm	LiF	685.13	10.76	
			685.77	1.3	12.06
	20 nm	LiF	685.16	8.21	
			685.64	0.95	9.16
O_2/N_2 (25:75)	0 nm	LiF	685.01	1.01	
		CF_3	688.58	2.01	3.02
	10 nm	LiF	685.05	9.72	
		CF_3	688.55	1.63	11.35
	20 nm	LiF	685.03	9.37	
		CF_3	688.38	1.3	10.67
Li + electrolyte + O_2		LiF	685.3	1.4	
		CF_3	689.08	7.04	8.44

Supplemental Table 6: Li 1s peak for SEI formed in O_2, Ar, and N_2 at various sputter depths. These shifts in peak position for the SEI in Ar environment may indicate heterogeneity in composition.

Environment	Depth	Position (eV)	%At Conc
Ar	0 nm	55.03	13.63
	10 nm	55.61	41.15
	20 nm	54.82	48.35
O_2	0 nm	54.28	23.66
	10 nm	55.1	42.49
	20 nm	55.11	45.94
N_2	0 nm	55.23	15.99

	10 nm	55.23	45.98
	20 nm	54.81	51.83
O_2/N_2 (25:75)	0 nm	55.36	19.49
	10 nm	55.39	46.13
	20 nm	55.32	48.29
Li pristine		55.89	21.79
Li + electrolyte + O_2		55.56	18.02
		54.74	8.81

Supplemental Table 7: Peaks in the O 1s spectra for SEI formed in O_2, Ar, and N_2 at various sputter depths. Li_2O can be seen for all samples ~ 529 eV.

Environment	Depth	Assignment	Position (eV)	%At Conc	%Total
Ar	0 nm	Carbonates/carbonyl	531.36	18.52	
		C-O	533.07	3.54	22.06
	10 nm	Li_2O	528.98	1.52	
		Carbonates/carbonyl	531.76	16.92	
		C-O	532.85	6.13	24.57
	20 nm	Li_2O	528.32	4.45	
		Carbonates/carbonyl	531.17	18.38	
		C-O	532.83	2.6	25.43
O_2	0 nm	Carbonates/carbonyl	531.02	26.4	
		C-O	533.23	0.94	27.34
	10 nm	Li_2O	529.14	4.73	
		LiOH	531.91	28.15	32.88
	20 nm	Li_2O	529.23	6.96	
		LiOH	532.02	26.42	33.38
N_2	0 nm	Carbonates/carbonyl	531.52	18.58	
		C-O	533.25	2.47	21.05
	10 nm	Li_2O	528.49	1.93	
		Carbonates/carbonyl	531.41	20.21	
		C-O	532.45	5.34	27.48
	20 nm	Li_2O	528.45	6.68	
		Carbonates/carbonyl	531.39	18.7	
		C-O	532.6	3.44	28.82
O_2/N_2 (25:75)	0 nm	Carbonates/carbonyl	531.7	17.88	
		C-O	533.15	5.16	23.04
	10 nm	Li_2O	528.45	4.01	
		Carbonates/carbonyl	531.38	21.25	
		C-O	533.1	3.12	28.38
	20 nm	Li_2O	528.3	5.45	
		Carbonates/carbonyl	531.31	21.23	
		C-O	533.4	1.93	28.61
Li pristine		Li_2O	529.34	1.98	
		Carbonates/carbonyl	531.2	1.54	
		C-O	532.55	15.86	19.38
Li + electrolyte + O_2		Carbonates/carbonyl	531.39	13.24	
		LiOH/S=O	532.27	5.19	
		C-O	533.1	10.64	29.07

Supplemental Table 8: N 1s peak for SEI formed in O_2, Ar, and N_2 at various sputter depths. The peaks are reduced, at lower binding energies, compared that of a $TFSI^-$ salt anion, indicating that decomposition products such as $-NSO_2CF_3$ fragments, $-NSO_x$ or even Li_3N may contribute to the SEI.

Environment	Depth	Position (eV)	%At Conc
Ar	0 nm	398.16	1.17
	10 nm	399.28	0.96
	20 nm	398.59	0.88
O_2	0 nm	398.05	0.32
	10 nm	398.84	0.3
	20 nm	399.08	0.27
N_2	0 nm	398.57	0.74
	10 nm	398.65	0.6
	20 nm	398.47	0.6
O_2/N_2 (25:75)	0 nm	398.33	2.18
	10 nm	398.81	1.1
	20 nm	398.69	0.96
Li + electrolyte + O2		398.2	0.26
		399.76	1.18

Supplemental Table 9: Peaks in the S 2p spectra for SEI formed in O_2, Ar, and N_2 at various sputter depths. The S 2p peaks manifest as doublets, although some peaks were difficult to deconvolute. Li_2S can be seen for all samples, ~160-162 eV, with larger relative atomic conc in Ar and N_2 samples.

Environment	Depth	Assignment	Position (eV)	%At Conc	%Total
Ar	0 nm	S=O	166.72	0.38	
		S=O	168.78	1.34	1.72
	10 nm	Li_2S	160.82	0.45	
		Li_2S	162.22	0.5	
		Li_2SO_3	163.57	0.15	
		Li_2SO_3	164.59	0.08	
		S=O	167.61	0.24	
		S=O	169.33	0.81	2.23
	20 nm	Li_2S	160.14	0.52	
		Li_2S	161.41	0.45	
		Additional decomp products	162.93	0.23	
		S=O	166.92	0.26	
		S=O	168.63	0.52	1.98
O_2	0 nm	S=O	166.19	0.05	
		S=O	168.17	0.75	0.8
	10 nm	Li_2S	160.49	0.16	
		Li_2S	161.87	0.23	
		S=O	167.58	0.17	
		S=O	169.87	0.17	0.73
	20 nm	Li_2S	160.77	0.33	
		Li_2S	162.25	0.07	
		S=O	167.6	0.09	
		S=O	169.74	0.24	0.71
N_2	0 nm	S=O	166.91	0.31	
		S=O	168.87	0.92	1.23
	10 nm	Li_2S	160.32	0.43	
		Li_2S	161.67	0.29	
		Li_2SO_3	162.95	0.2	
		Li_2SO_3	164.2	0.16	
		S=O	167.25	0.32	

		S=O	169.34	0.68	2.09
	20 nm	Li_2S	160.16	0.19	
		Li_2S	161.25	0.71	
		S=O	167.26	0.24	
		S=O	169.1	0.37	1.51
O_2/N_2 (25:75)	0 nm	Li_2S	161.96	0.28	
		S=O	167.27	0.6	
		S=O	168.83	0.94	1.82
	10 nm	Li_2S	160.3	0.35	
		Li_2S	161.74	0.37	
		Additional decomp products	163.22	0.35	
		S=O	167.08	0.31	
		S=O	168.73	0.68	2.06
	20 nm	Li_2S	160.15	0.32	
		Li_2S	161.58	0.58	
		Additional decomp products	163.17	0.34	
		S=O	167	0.11	
		S=O	168.55	0.53	1.88
Li + electrolyte + O_2		S=O	167.18	0.37	
		S=O	169.43	2.74	3.11

(1) Aurbach, D. The Correlation Between Surface Chemistry, Surface Morphology, and Cycling Efficiency of Lithium Electrodes in a Few Polar Aprotic Systems. *J. Electrochem. Soc.* **1989**, *136* (11), 3198. https://doi.org/10.1149/1.2096425.

(2) Peled, E.; Golodnitsky, D.; Ardel, G. Advanced Model for Solid Electrolyte Interphase Electrodes in Liquid and Polymer Electrolytes. *J. Electrochem. Soc.* **1997**, *144* (8), 202–210.

(3) West, A.; Irvine, J.; Sinclair, D. Electroceramics : Characterization by Impedance Spectroscopy. *Adv. Mater.* **1990**, *2* (3), 132–138. https://doi.org/093S-9648~90/0303-0132.

(4) Aurbach, D.; Cohen, Y. S. Identification of Surface Films on Electrodes in Non-Aqueous Electrolyte Solutions: Spectroscopic, Electronic and Morphological Studies. In *Lithium-Ion Batteries - Solid-Electrolyte Interphase*; Balbuena, P. B., Wang, Y., Eds.; Imperial College Press, 2004; pp 70–139.

(5) Macdonald, J. R.; Kenan, W. R. *Impedance Spectroscopy: Emphasizing Solid Materials and Systems*; Wiley: New York, 1987.

(6) Sharon, D.; Hirshberg, D.; Afri, M.; Garsuch, A.; Frimer, A. A.; Aurbach, D. Lithium-Oxygen Electrochemistry in Non-Aqueous Solutions. **2015**, *67056*, 508–520. https://doi.org/10.1002/ijch.201400135.

(7) Assary, R. S.; Lu, J.; Du, P.; Luo, X.; Zhang, X.; Ren, Y.; Curtiss, L. A.; Amine, K. The Effect of Oxygen Crossover on the Anode of a Li-O2 Battery Using an Ether-Based Solvent: Insights from Experimental and Computational Studies. *ChemSusChem* **2013**, *6*, 51–55.

(8) Aurbach, D.; Granot, E. The Study of Electrolyte Solutions Based on Solvents from the “Glyme” Family (Linear Polyethers) for Secondary Li Battery Systems. *Electrochim. Acta* **1997**, *42* (4), 697–718. https://doi.org/10.1016/S0013-4686(96)00231-9.

(9) Camacho-Forero, L. E.; Balbuena, P. B. Elucidating Electrolyte Decomposition under Electron-Rich Environments at the Lithium-Metal Anode. *Phys. Chem. Chem. Phys.* **2017**, *19* (45), 30861–30873. https://doi.org/10.1039/c7cp06485c.